ACS APPLIED NANO MATERIALS

www.acsanm.org

Article

Coupling of Triboelectric and Piezoelectric Effects in Nafion-Containing Polyvinylidene Fluoride: Lead Zirconium Titanate Nanofiber-Based Nanogenerators for Self-Powered Systems

Saira Bano, Bablesh Gupta, Satinder K. Sharma, and Ranbir Singh*

Cite This: *ACS Appl. Nano Mater.* 2024, 7, 15425–15437

Read Online

ACCESS | Metrics & More | Article Recommendations | Supporting Information

ABSTRACT: The rapid advancement of nanocomposite materials for coupled triboelectric and piezoelectric nanogenerators (TENG-PENG) has attracted considerable attention due to efficient mechanical energy harvesting in portable and self-powered systems. However, challenges persist due to the nonuniform distribution of guest materials within nanocomposites, resulting in limited surface potential and polarization properties. Here, we demonstrated the incorporation of Nafion into poly(vinylidene fluoride):lead zirconium titanate (PVDF:PZT) hybrid nanofibers, substantially enhancing the β phase. The surface potential of PVDF:PZT increased to 86 mV, representing a 21% increase over untreated PVDF, while stimulated PVDF:PZT-N hybrid nanofibers show a notable boost of ~175 mV, increasing to 146% compared to PVDF. The hybrid PVDF:PZT-N exhibits a storage modulus of ~306 Pa and electrospun hybrid nanofibers displays an elastic limit of ~1.48 MPa. Furthermore, the efficacy of the PVDF:PZT-N nanofibers is validated through a comparative analysis between engineered single- and double-dielectric layered TENG-PENG devices, producing maximum output currents and voltages of ~7 μA and ~40 V, respectively. These TENG-PENG devices have demonstrated their potential to illuminate multiple light-emitting diodes and digital LED display boards. Overall, the incorporation of Nafion into PVDF:PZT nanofibers significantly enhances the output performance of synergistically integrated PENG and TENG systems, offering promising advancements in mechanical energy harvesting and self-powered electronic devices.

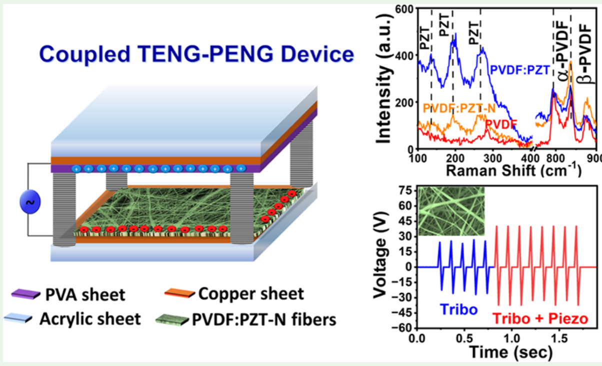

KEYWORDS: *poly(vinylidene fluoride), lead zirconium titanate, triboelectric nanogenerator, piezoelectric nanogenerator, electrospun, nanofibers, nafion*

1. INTRODUCTION

Electronic devices, ranging from electric cars to various smart gadgets, continue to proliferate rapidly leading to a widespread and increasing demand for charging solutions.[1] Parallelly, the demand for portable power sources and electronic waste is also booming. Amidst the escalating energy crisis, it is crucial to explore alternative routes to eliminate reliance on non-renewable energy sources and the usage of toxic batteries.[2] The emerging accessible technologies are triboelectric and piezoelectric nanogenerators.[3] Recently, researchers have extended their focus to harvest ubiquitous kinetic energy from chalcohalide nanowires that exhibit exceptional electromechanical and piezoelectric properties, making them ideal for their use in nanogenerators. These nanogenerators can efficiently convert mechanical energy from diverse sources, such as acoustic waves, airflow, and body movements into electricity. Additionally, they are capable of detecting ultrasonic waves and low-frequency vibrations.[4,5] Nanofibers-based coupled triboelectric nanogenerators (TENGs) and piezoelectric nanogenerators (PENGs) are also emerging technologies that transform mechanical energy into electrical power.[6] Considering their affordable fabrication costs and adequate energy conversion efficiency, TENGs and PENGs are attracting significant attention. These devices perform through the coupling effect of contact electrification and electrostatic induction.[7] Triboelectric nanofiber materials have the capacity to generate charges on their surface while coming in close proximity with oppositely charged dielectric materials.[8] However, piezoelectric nanofiber materials perform their role when pressure is exerted over them, where electric charges develop due to electric polarization produced by a mechanical strain.[9] Also, it has been observed that a nanofiber-based single

Received: April 20, 2024
Revised: June 1, 2024
Accepted: June 7, 2024
Published: June 25, 2024

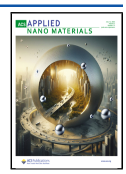

nanogenerator, which are made up of polymer materials, could transit into the couple stages of TENG and PENG due to their excessive degree of bending and intrinsic flexibility.[10]

The poly(vinylidene fluoride) (PVDF)-based polymer is most commonly used in flexible triboelectric and piezoelectric devices that exhibit outstanding energy-harvesting potential.[11] PVDF $(-CH_2-CF_2-)_n$ is a semicrystalline material whose piezoelectric property depends upon the dipoles between the C−H and C−F bonds.[12] Generally, PVDF can crystallize in two polymorphs, identified as α and β phases.[13] The α phase is characterized by trans−gauche−trans−gauche′ (TGTG′) conformation, whose dipole moments are aligned in an antiparallel way, and the β phase is characterized by all-trans (TTTT) conformation.[14] The β phase is more stable as it endures a large electric field due to the applied mechanical deformation.[15,16] However, under typical conditions, PVDF is severely constrained by factors like non-polar phase, poor dielectric permittivity, and low mechanical strength.[17] To impede these constraints, high-dielectric dopants are added with PVDF to develop an efficient composite material with improvized dielectric breakdown, dielectric constant, and flexibility.[18,19] Several studies have been explored to design an efficient composite material with PVDF by using different types of dopants such as lead zirconium titanate (PZT), zinc oxide, graphene nanosheets, and cobalt chloride.[20,21] Particularly, high dielectric constant PZT incorporated into PVDF (PVDF:PZT) improves the surface charge density, dielectric properties, charge-trapping capability, and outstanding mechanical stability.[22,23] The inclusion of PZT serves as a catalyst, prompting nucleation during the curing process and fostering increased crystallization through electrostatic attraction.[24] In PVDF:PZT composites, PZT induces local stress between the interface of PZT and PVDF, tend to significantly enhance the stress-induced polarization in the polymer matrix, and exhibited better piezoelectric properties compared to bare PVDF.[25] However, the hydrophobic properties of PVDF with low density (1.78 g/cm^3) and the hydrophilic nature of PZT with high density (7.45 g/cm^3) creates a limiting factor for the complete dispersion of PZT into PVDF. Inevitably, due to large density difference between the PVDF and PZT components of composite, it produces high agglomeration and low dispersion.[26−29] Thus, weak interfacial interactions between PZT and PVDF reduces the output power and stability of TENG-PENG.[30] Hence, it is crucial to produce a well-dispersed homogeneous phase of the PVDF:PZT composite for outstanding results. Moreover, a significant enhancement in dielectric properties of PVDF can be acheived by the addition of PZT in the presence of organically modified additives.[31]

In this work, we incorporated Nafion as an additive into PVDF:PZT composite solution to form PVDF:PZT-N hybrid electrospun nanofibers. The unique hydrophilic and hydrophobic functionality of Nafion resulted in a uniformly dispersed phase of PVDF:PZT-N hybrid nanofibers, which helps to improve the triboelectric and piezoelectric performance. Additionally, a comparative study of engineered TENG-PENG devices utilizing a single dielectric and double dielectric layer was conducted. In order to enhance the triboelectric and piezoelectric effects of double dielectric layer TENG-PENG device, poly(vinyl alcohol) (PVA) is integrated as an electropositive layer with a top-side copper electrode. The properties of the synthesized nanofibers were characterized by using X-ray diffraction (XRD), field-emission scanning electron microscopy (FE-SEM), Raman spectroscopy, Kelvin probe force microscopy (KPFM), and universal testing machines (UTM).

2. EXPERIMENTAL SECTION

2.1. Materials. PVDF pellets, acetone, and *N*,*N*-dimethylformamide (DMF) solvents of commercial grade were procured from Sigma-Aldrich. Nafion and PVA were supplied by Alfa Aesar, while PZT powder was purchased from Nanoshel, India.

2.2. Fabrication of Nafion-Incorporated PVDF:PZT Nanofibers. PVDF pellets of Mw −180,000 were first dissolved in a DMF solvent and acetone (4:1) to prepare a homogeneous solution of 24 wt % and stirred for 9 h at 60−70 °C. Further, PZT powder of different fractions (1.4, 4.8, 9.6, and 14.4 wt %) was added into the PVDF solution and stirred for 1 h to form a homogeneous mixture. Additionally, Nafion with different volume concentrations (20, 40, 60, and 100 μL) was added dropwise to the PVDF:PZT solution and stirred for 1 h. Finally, the prepared solution was loaded into a syringe pump and placed 45 cm away from the collecting cylinder for electrospinning. The nanofibers were deposited with a feed rate of 2 mL h^{-1} in the presence of high voltage of 17 kV. Electrospun PZT:PVDF-N nanofibers were collected on an aluminum foil wrapped over a collecting cylinder.

2.3. TENG-PENG Device Fabrication. The device fabrication relies on the vertical contact separation mode. First, electrospun PVDF nanofibers, PVDF:PZT composite nanofibers, and PVDF:PZT-N hybrid nanofibers were directly collected from aluminum foil which was wrapped on the collecting cylinder. Then, the single-dielectric TENG-PENG device was fabricated by assembling the PVDF:PZT-N nanofiber mat serving as the first dielectric layer placed on conductive copper sheets. Another copper sheet, which acted as the upper electrode was attached to the top side. Two acrylic sheets were deployed on both copper sheets to assemble the positive and negative copper electrodes. Similarly, single-dielectric TENG-PENG devices were fabricated using PVDF nanofibers and PVDF:PZT composite nanofibers. Moreover, for the double-dielectric TENG-PENG device, a PVA thin film as a second dielectric layer was coated on an upper copper sheet to serve as a positive triboelectric layer and mounted over the PVDF:PZT-N nanofiber mat.

2.4. Morphological and Structural Characterization. The morphological analysis of PVDF nanofibers, PVDF:PZT composite nanofibers, and PVDF:PZT-N hybrid nanofibers was done using an FE-SEM (Zeiss Gemini 500, Carl Zeiss Microscope) at an acceleration voltage of 5 kV. The crystalline structure was obtained using X-ray diffraction (SmartLab X-ray Diffractometer) at a scan rate of 1° min^{-1}. Raman signal acquisition was performed (LabRAM Hr evolution) using a 532 nm incident laser with a 100× objective lens. The d_{33} piezoelectric constant was measured using a YE2730A piezometer (APC International, Ltd).

2.5. Kelvin Probe Force Microscopy (KPFM). KPFM measurement was conducted using a Bruker multimode system (Dimension ICON PT) under ambient conditions. The non-contact mode was operated through a Co−Cr-coated conducting tip (cantilever frequency: ∼75 kHz, nominal spring constant: 3 N m^{-1}, and curvature size: 35 nm) to measure the surface potential and topology of the electrospun nanofibers. Further, Nasoscope analysis software was utilized to calculate the surface potential distribution along multiple line profiles.

2.6. Electrical Characterization. The two ends of the conductive copper sheet were connected to the two electrodes of Kethley 4200ASCS, which were used to measure the output current. The ouput voltage was measured using high-speed digital storage oscilloscope (Agilent Technologies).

2.7. Rheological and Tensile Strength Characterization. Rheological measurement of PVDF:PZT-N, PVDF:PZT, and PVDF in molten state was carried out using a modular compact rheometer (Anton Paar), equipped with a conical plate geometry (diameter = 40 mm and gap = 1 mm). Tensile strength measurement was performed using a UTM (Tinius Olsen) to compare the strength of the

https://doi.org/10.1021/acsanm.4c02292
ACS Appl. Nano Mater. 2024, 7, 15425−15437

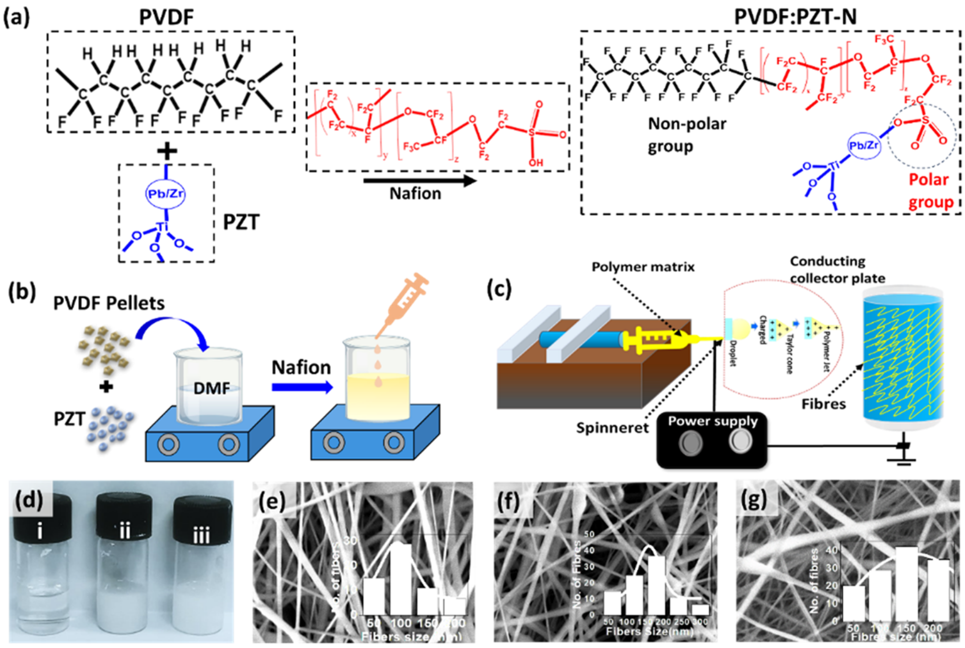

Figure 1. (a) Chemical structures of the materials used and interactions exist in Nafion-incorporated PVDF:PZT, (b) synthesis process of the precursor solutions, and (c) electrospinning of PVDF:PZT-N nanofibers. (d) Stable solution of (i) PVDF, (ii) PVDF:PZT, and (iii) PVDF:PZT-N. FE-SEM images with Gaussian fit on nanofibers of various sizes (e) PVDF, (f) PVDF:PZT, and (g) PVDF:PZT-N.

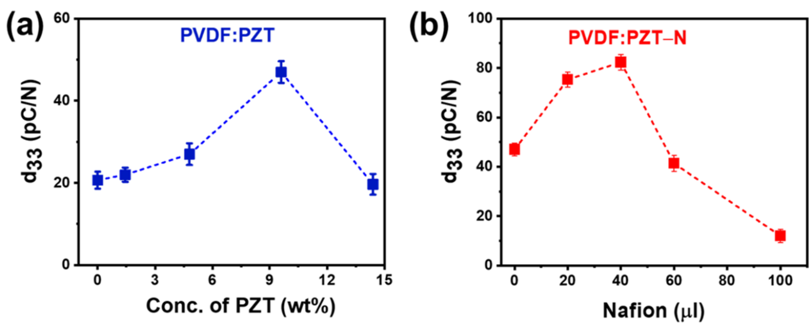

Figure 2. Piezoelectric coefficient (d_{33}) of fabricated PVDF:PZT composite nanofibers corresponding to various concentrations of (a) PZT (0, 1.4, 4.8, 9.6, and 14.4 wt %) and (b) Nafion (0, 20, 40, 60, and 100 μL).

PVDF:PZT-N hybrid nanofibers with PVDF:PZT and bare PVDF nanofibers. The sample size (2 mm × 30 mm) was fixed between a frame holder with a gauge length of 3 cm, strain rate of 1 mm min^{-1}, and using a load cell of 10 N.

3. RESULTS AND DISCUSSION

Figure 1a illustrates the molecular structures of PVDF, PZT, and Nafion along with their interactions. The introduction of Nafion into PVDF:PZT arises the polar interactions between PZT and Nafion, while nonpolar interactions between PVDF and Nafion. These interactions emerge due to the Nafion contains perfluoroalkyl backbones and sulfonic groups, which exhibit hydrophobic and hydrophilic properties.[32] The unique amphiphilic properties of Nafion enabled hydrophilic interactions between PZT and the sulfonic group of Nafion, including hydrophobic interactions between the PVDF chain and perfluoroalkyl backbones of Nafion. Figure 1b schematically shows the preparation of Nafion-incorporated PVDF:PZT hybrid solution. PVDF:PZT composite solutions with varying concentrations of PZT are shown in Figure S1a. Thereafter, Nafion at different concentrations was added to the well-dispersed PVDF:PZT composite to form a PVDF:PZT-N hybrid solution, as shown in Figure S1b. In the electrospinning process, the synthesized solution is ejected from a capillary nozzle and dispersed into the nanofibers under the influence of a strong electric field, as illustrated in Figure 1c. The stable solutions of PVDF, including PVDF:PZT, and PVDF:PZT-N for the optimized concentrations of PZT and Nafion are shown in Figure 1d. Moreover, the excellent dispersion of PZT in the PVDF:PZT-N hybrid solution is due to the bond interaction of Nafion with the lead oxide (PbO) molecules of PZT, as shown by Fourier transform infrared (FTIR) spectroscopy in Figure S2a, and the enlarged plot in Figure S2b.

3.1. Morphological Analysis. The FE-SEM images of PVDF, PVDF:PZT, and PVDF:PZT-N nanofibers, along with the average size distributions, are shown in Figure 1e−g. The pure PVDF nanofibers exhibited diameters in the range of 50 to 200 nm with an average fiber diameter of 100 nm. To optimize the PVDF:PZT composite nanofibers, the concentration of PZT was varied from 4.8 to 14.4 wt %, as shown in SEM images (Figure S3b−d), with higher resolution in Figure S3f−h. The high concentration of PZT in the PVDF:PZT composite nanofiber images clearly shows the aggregated PZT. The PVDF:PZT images reflect the non-uniform distribution of

https://doi.org/10.1021/acsanm.4c02292
ACS Appl. Nano Mater. 2024, 7, 15425−15437

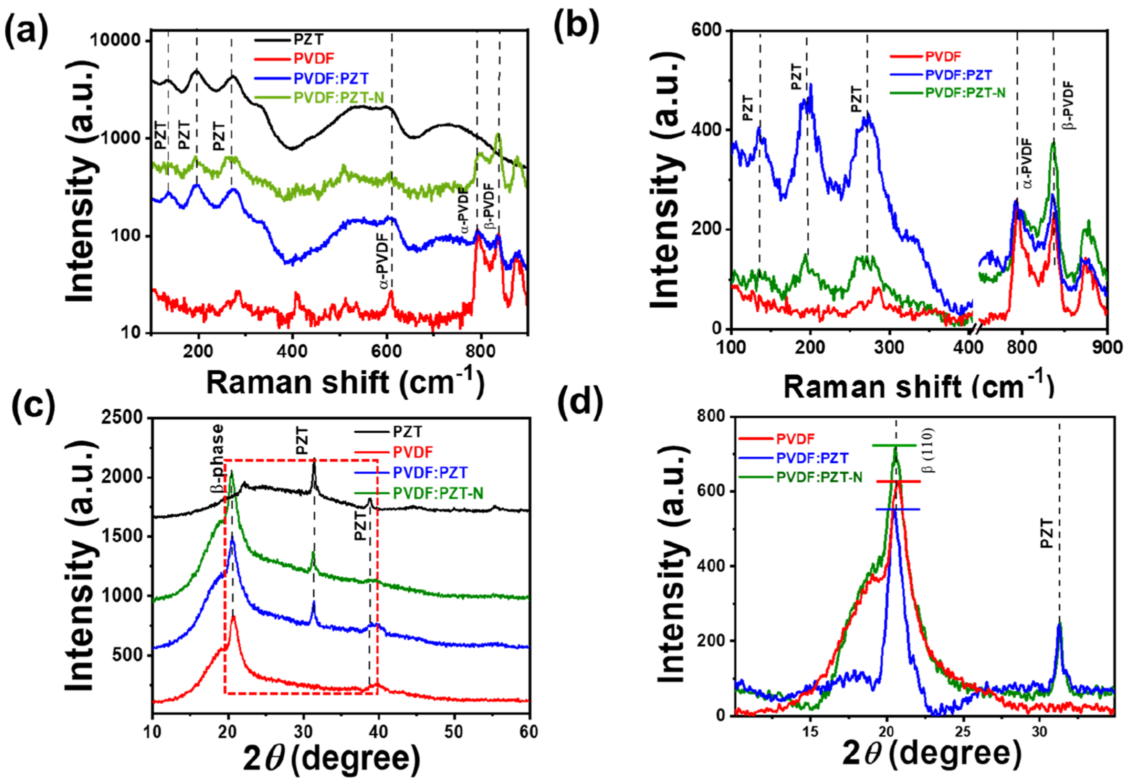

Figure 3. (a) Raman spectra of PVDF, PVDF:PZT, and PVDF:PZT-N nanofibers along with only PZT film. (b) Zoomed-in Raman spectra of PVDF, PVDF:PZT, and PVDF:PZT-N nanofibers. (c) XRD spectra of PZT, PVDF, PVDF:PZT, and PVDF:PZT-N with (d) zoomed data for the (110) peak.

PZT within the nanofibers, and the nanofiber size varied from 50 to 300 nm with an average fiber diameter of 180 nm. The primary reason for larger aggregates of PZT in the PVDF:PZT nanofiber is a nonuniform distribution of PZT, which produced a greater impact force during electrospinning, when hovering toward the fiber collection roller.[33] The morphology of the PVDF:PZT-N hybrid nanofiber shows the size in the range of 50 to 200 nm, which exhibits an average fiber size of 150 nm without aggregated PZT. The crucial function of Nafion involves reducing the agglomeration in the PVDF:PZT-N composite by adjusting the surface energy and density disparities between PVDF and PZT.[34] The FE-SEM images of the fabricated PVDF:PZT-N hybrid nanofibers at different concentrations of Nafion are shown in Figure S4a−c.

The d_{33} coefficient was assessed for the maximum piezoelectric output when subjected to applied stress. Figure 2a presents the d_{33} measurement of the PVDF:PZT composite nanofibers with different PZT concentrations. The PZT concentration of 9.6 wt % exhibits a maximum d_{33} value of 48 pC/N. This is due to the inherent superior piezoelectric property and the mechanical strength of PZT as compared to PVDF, which enhanced the alignment of polarizable dipoles within the PVDF:PZT composite.[35] However, increasing the PZT concentration led to decrease in the d_{33} value. The PVDF:PZT composite solution was found to be optimized at 9.6 wt % PZT, in which Nafion was further added in various concentrations to form a PVDF:PZT-N solution. The PVDF:PZT-N nanofibers exhibited an impressive d_{33} value of 81 pC/N with the addition of 40 μL of Nafion; further increase in the Nafion concentration leads to a non-linear decrease in d_{33}, as depicted in Figure 2b. Nafion additives integrated into the PVDF:PZT composites not only improve the piezoelectric effect but also exert a substantial influence on crystallinity through electrostatic interactions. Therefore, Nafion, as a conductive additive in the PVDF:PZT-N hybrid nanofibers, is a stress-reinforcing agent that enhances the force distribution to the internal crystal phase.[36]

3.2. Raman Analysis. Raman analysis was employed to examine the structural changes and phase transformations in the PVDF:PZT-N hybrid nanofibers and compared with untreated PVDF and PVDF:PZT composite nanofibers. In Figure 3a, the spectra of bare PVDF nanofibers illustrate the structural characteristics of the material. Two distinct para-electric α phase features are observed at approximately 608 and 793 cm^{-1}. Additionally, the presence of the β phase in PVDF is evident at approximately 837 cm^{-1}, corresponding to the out-of-phase combination of the CF_2 stretching mode and CH_2 rocking.[37] This particular β phase configuration is known to contribute the enhancement of piezoelectric properties. The α phase peak intensity is predominantly observed in the bare PVDF nanofibers. Following the addition of PZT to PVDF, the PVDF:PZT composite spectra prominently exhibited distinct PZT peaks at 136, 191, and 272 cm^{-1}. Moreover, a noticeable enhancement in the β phase peak dominated over the α phase peak. The Raman bands below 150 cm^{-1} are known as the exterior modes of the PZT material; in particular, they are connected to the lead-lattice modes. On the other hand, modes above 150 cm^{-1} reflect internal bands like torsion, bending, and stretching.[38] Moreover, upon the introduction of Nafion in the PVDF:PZT composite, we observed a reduction in the intensity of the PZT peaks compared to the peak intensity of the α and β phases in bare PVDF nanofibers. Remarkably, the intensity of the β phase peak was significantly enhanced after Nafion incorporation. This occurred because of the hydrated

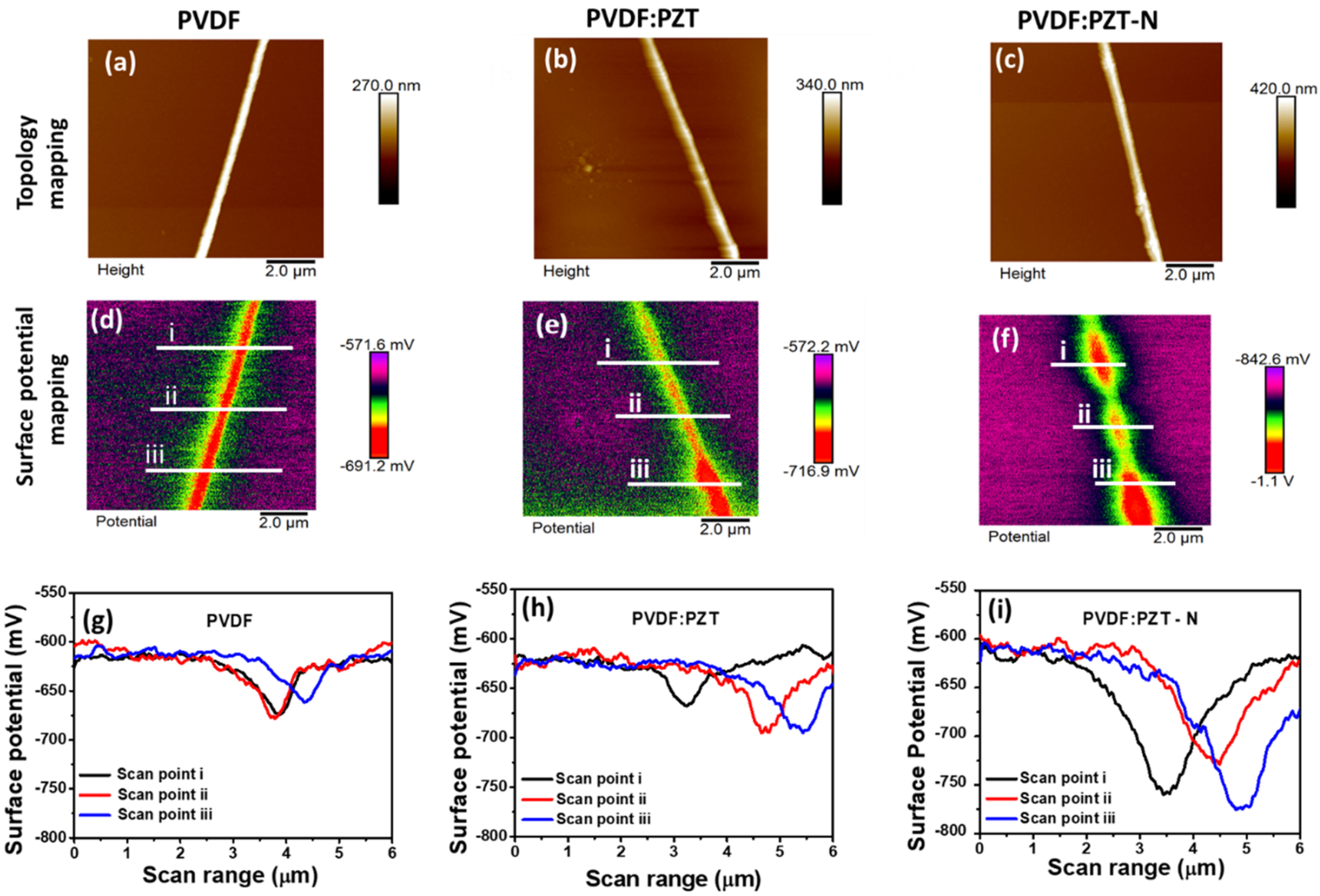

Figure 4. KPFM measurement of PVDF, PVDF:PZT, and PVDF:PZT-N representing (a−c) topology scan image, (d−f) surface potential mapping, and (g−i) multiple line profiles of surface potential distribution.

sulfonated groups in the PVDF:PZT-N nanofibers, which improved the β/α peak intensity ratio of ∼1.44. The formidable dielectric characteristics of PZT particles increase the polarization of PVDF upon exposure to an electric field during electrospinning of nanofibers.[39] Additionally, Raman mapping was conducted at ten distinct locations across a 10 × 10 μm^2 area to assess the signal uniformity of PVDF, PVDF:PZT, and PVDF:PZT-N, as illustrated in Figure S5. The reduced intensity of the PZT peaks observed for PVDF:PZT-N signifies the homogeneous distribution of PZT.

3.3. XRD Analysis. The polymorphic characteristic of the PVDF, pristine PZT, PVDF:PZT, and PVDF:PZT-N materials was investigated using XRD data, as shown in Figure 3c (zoomed data in Figure 3d). The diffraction peaks of PZT are typically observed at 31° and 38°.[40] In bare PVDF, a prominent diffraction peak is observed at 2θ = 20.3°, which corresponds to the (110) reflection plane of the polar β phase. This peak reflects the Bragg diffraction of the β phase, which is associated with all-trans conformations.[41] However, the β phase peaks for PVDF:PZT are at the same location, but the intensity of the peak dropped, which indicates that the presence of the PZT peak dominates and suppresses the β phase of PVDF. This suppression may be attributed to an increase in the number of aggregated PZT crystals within the PVDF:PZT composite. Moreover, with the incorporation of Nafion into PVDF:PZT, the intensity of the β phase peak was significantly enhanced. This enhancement is attributed to interaction between PZT and sulfonate groups of Nafion, which reduce coagulation and provide better dispersion of PZT within PVDF:PZT-N.[42] The interaction between PVDF, PZT, and Nafion also increases the crystallinity of the composite and may cause the polymer chains to become entrenched in the crystalline β phase, promoting polarization enhancement.[43] Additionally, the broad hump that arises in each XRD plot corresponds to the peak of the glass, as shown in Figure S6.

3.4. KPFM Analysis. The enhancement in the synergetic effect of the triboelectric and piezoelectric properties was investigated by studying the surface potential of the nanofibers with KPFM measurement. Initially, we scanned an area of 10 × 10 μm^2 to measure the topology of the pure PVDF, PVDF:PZT, and PVDF:PZT-N nanofibers, as shown in Figure 4a−c. The measured surface potentials of each aforementioned nanofibers are illustrated in Figure 4d−f. The change in the surface potential of the bare PVDF nanofibers, with an approximate value of ∼71 mV, slightly increases to ∼86 mV after doping with PZT, indicating a 21% increase compared to pure PVDF nanofibers. Moreover, the change in the surface potential of PVDF:PZT-N significantly reaches ∼175 mV, marking a remarkable 103% increase compared to the PVDF:PZT composite and a substantial 146% increase compared to the bare PVDF nanofibers. This indicates a notable enhancement in the uniformity of the β phase after the introduction of PZT and Nafion. The distribution of the surface potential along a line profile at different positions is illustrated in Figure 4g−i. The significant surface potential

https://doi.org/10.1021/acsanm.4c02292
ACS Appl. Nano Mater. 2024, 7, 15425−15437

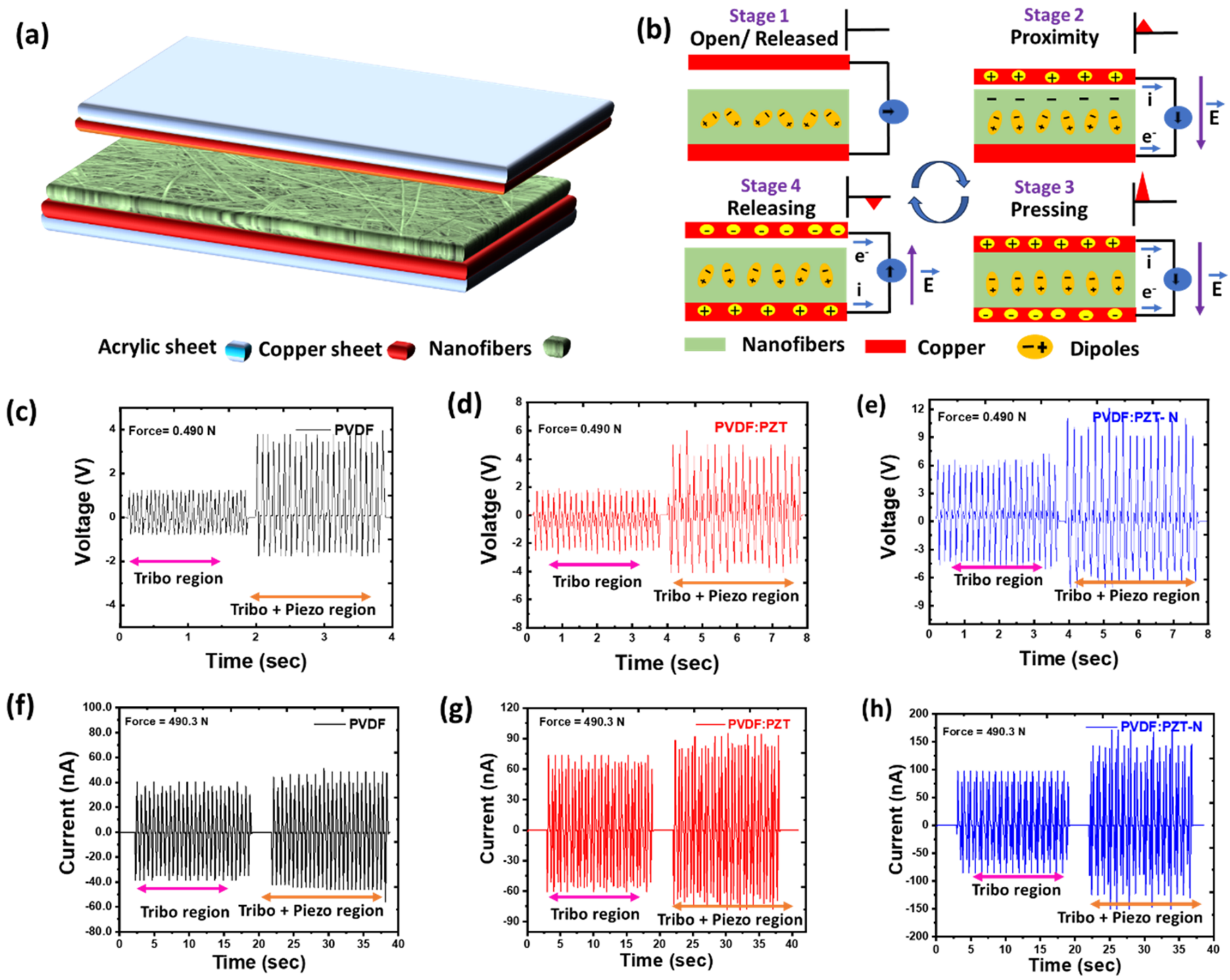

Figure 5. Single dielectric layer TENG-PENG device (a) structure, (b) working principle, (c−e) voltage measurement, and (f−h) output current for PVDF, PVDF:PZT and PVDF:PZT-N composite nanofibers.

observed for PVDF:PZT-N reflects a substantial induced electric field that boosts the polarization of the dielectric nanofibers. The high surface potential observed in PVDF:PZT-N signifies a large induced electric field, which contributes to the improved polarization of the dielectric materials. This enhancement reflects the improved homogeneity of the β phase.[44] Moreover, this outstanding surface potential supports superior enhancement of surface charges in PVDF:PZT-N. The increased polarizability facilitates more surface charge generation, thus enhancing the charge-trapping capability of the nanofibers.[45] The effective performance of the TENG-PENG device is significantly influenced by the surface potential of the contact materials, where materials with a notably negative surface potential favor charge acquisition, and vice versa.[46,47] Consequently, the PVDF:PZT-N configuration enables the accumulation of additional charges under an electric field, making it an excellent choice for coupled TENG-PENG nanogenerators.

3.5. Electrical Characterization and Analysis. To explore the triboelectric and piezoelectric properties of the PVDF:PZT-N nanofibers, we fabricated two individual TENG-PENG device structure, one designed with single dielectric layer and another with double dielectric layers. In the single dielectric layer TENG-PENG structure, a copper sheet was attached to PVDF:PZT-N nanofiber mat, which was vertically positioned against another copper sheet, as depicted in Figure 5a. The PVDF:PZT-N hybrid nanofibers are characterized by their electronegativity and exhibit a robust affinity for electron acquisition, while the electropositive copper layer has a propensity to release electrons.[48] The working mechanism of the single dielectric layer TENG-PENG device is illustrated in different stages of a single-loop cycle, as shown in Figure 5b. Stage 1 represents the initial phase, open/released state have open air space of ∼2.5 cm between the electropositive upper copper electrode and electronegative nanofiber layers. Consequently, there exist no potential difference, leading to no charge transfer. Stage 2 corresponds to gentle manual tapping, where the upper electropositive copper layers comes into close proximity to the electronegative nanofiber layers, triggering an opposite charge to emerge due to contact electrification, and electrostatic induction prompts few electrons to migrate from the bottom copper to the upper copper electrode, resulting in a small potential difference that produces a positive pulse.[49] After exerting mechanical pressure, the device enters into the pressing state or stage 3.[50] The upper electropositive copper electrode interfaces with the electro-

https://doi.org/10.1021/acsanm.4c02292
ACS Appl. Nano Mater. 2024, 7, 15425−15437

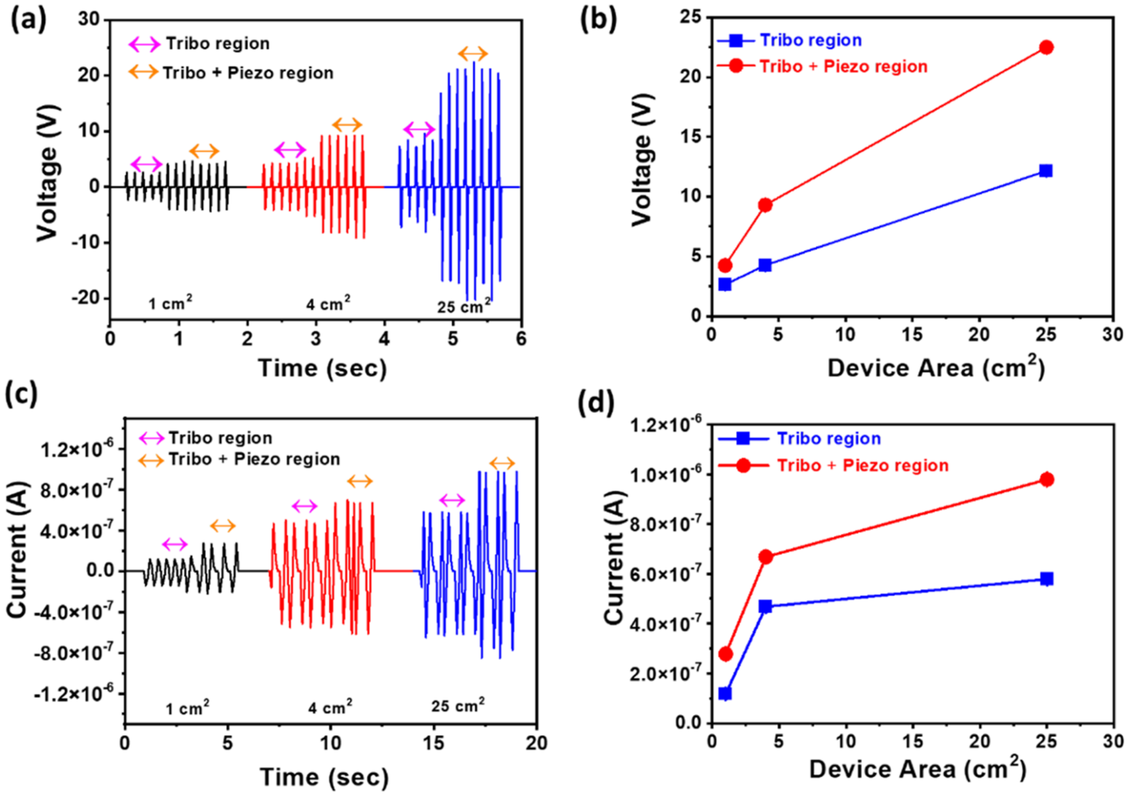

Figure 6. Area-dependent single-dielectric TENG-PENG device: (a) output voltage versus time and (b) maximum output voltage versus device area. (c) Output current versus time and (d) maximum output current versus device area.

negative nanofiber layers; hence, the piezoelectric effect becomes operative. Due to the applied pressure, stress is induced within the nanofibers. Hence, the dipoles of the nanofibers are properly aligned, consequently amplifying the potential difference, which facilitates the charge transfer from the bottom electrode to the upper electrode. Thus, it generates a high output pulse which get superimposed on the output pulse produced through only triboelectric effect. During the stage 4 or releasing state, electrostatic induction led to induce the electron flow between the two electrodes to equalize the potential difference, enabling charge transfer from the upper copper electrode to the bottom copper electrode through an external circuit, consequently generating a negative output pulse.[51] Further, charge neutralization occurs between the electrodes after complete separation from the triboelectric and piezoelectric effects.[52,53] Ultimately, the device returns to the initial stage or open/released state characterized by disoriented dipoles.[54] Figure 5c−e illustrates the output voltage waveform for the triboelectric effect in PVDF, PVDF:PZT , and PVDF:PZT-N nanofibers, respectively. These figures also depict the coupled triboelectric and piezoelectric effects under the same vertical applied force of 0.490 N, tapping frequency of 2 Hz, and constant area for all three single dielectric layer TENG-PENG.

The experimental results reveal notable enhancements in the output voltage when transitioning from the triboelectric region to the coupled triboelectric and piezoelectric (Tribo + Piezo) regions for different nanofiber-based devices. For the untreated PVDF nanofiber TENG-PENG, the output voltage experiences a 2.5-fold increment in the coupled triboelectric and piezoelectric regions compared to the solely triboelectric region. Similarly, the output voltage of the PVDF:PZT composite nanofiber device reaches 5 V in the coupled triboelectric and piezoelectric regions compared with the maximum of 2 V in the triboelectric region alone. Moreover, in PVDF:PZT composite nanofiber device, PZT is added as a high dielectric material, which enhances the output voltage compared to the bare PVDF nanofiber device. Generally, PZT has showed significantly higher electromechanical coupling factor and exceptionally good piezoelectric properties, resulting in greater conversion efficiency of mechanical stress into electrical current. Thus, the PVDF:PZT composite material can harness superior piezoelectric properties, thereby amplifying the voltage generated when subjected to mechanical deformation.[55] The PVDF:PZT-N nanofiber-based device demonstrates an output voltage of 6 V in the triboelectric region and 9 V in the coupled triboelectric and piezoelectric regions. Furthermore, the output current at an applied force of 490.3 N is determined for PVDF, PVDF:PZT, and PVDF:PZT-N, as shown in Figure 5f−h. It is notable that the electrical output performance was enhanced during the device conversion state from only triboelectric region to the coupled triboelectric and piezoelectric regions. As PVDF is a superior piezoelectric material, upon impacting complete mechanical pressure, the deformation in PVDF nanofibers allows easy electron flow through the external circuit for a shorter duration in response to the piezoelectric potential change. Further, the reinforcement of PZT corresponds to a high piezoelectric effect with an excellent dielectric constant, enhancing the output signal, while Nafion enhances the electrostatic interactions among the components of PVDF:PZT-N hybrid nanofibers. Thus, during the close proximity between the electropositive copper sheet and nanofiber layers, it responds to the triboelectric effect of low

https://doi.org/10.1021/acsanm.4c02292
ACS Appl. Nano Mater. 2024, 7, 15425−15437

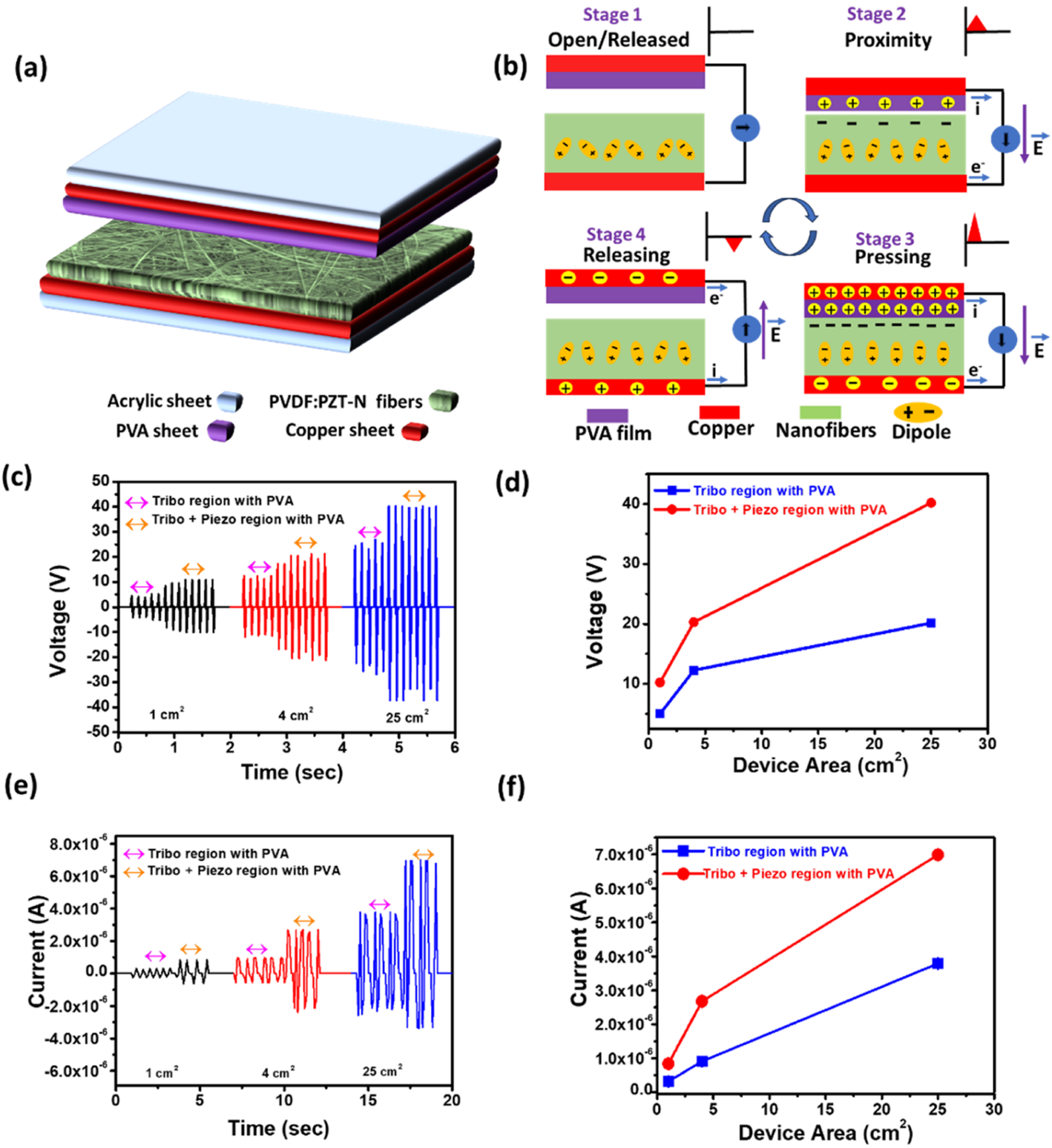

Figure 7. Double-dielectric layer area-dependent TENG-PENG: (a) device structure and (b) operational mechanism. (c) Output voltage, (d) maximum output voltage, (e) output current, and (f) maximum output current with respect to area.

voltage. However, upon exerting complete mechanical pressure, the device state converts from a triboelectric to coupled triboelectric and piezoelectric regions. The average output current of the untreated PVDF nanofiber device increased to 4×10^{-8} A in the coupled triboelectric and piezoelectric regions, compared to 3×10^{-8} A in the triboelectric region alone. For the PVDF:PZT composite nanofiber device, the output current increases from 7×10^{-8} A in the triboelectric region to 9×10^{-8} A in the coupled triboelectric and piezoelectric regions. Finally, the PVDF:PZT-N hybrid nanofiber device exhibit an increase in the output current from 1×10^{-7} A in the triboelectric region to 1.6×10^{-7} A in the coupled triboelectric and piezoelectric regions. Nafion is amphiphilic in nature, which enhances its binding properties between PVDF and PZT. Thus, the high ionic conductivity of Nafion due to the perfluorosulfonic acid group readily distributes the charges within the PVDF:PZT composites, amplifying the electric field produced within the

https://doi.org/10.1021/acsanm.4c02292
ACS Appl. Nano Mater. 2024, 7, 15425−15437

nanofibers when subjected to the applied mechanical stress.[56] The high mechanical strength and flexibility of Nafion improved the deformation of the PVDF:PZT-N hybrid nanofibers, facilitating easy charge generation and transportation, eventually enhances the piezoelectric output response.[57] These findings confirm the incorporation of Nafion enhances the triboelectric and piezoelectric responses of the PVDF:PZT-N nanogenerators compared to the bare PVDF. The effectiveness of the coupled TENG-PENG device also relies on the high surface potential and surface charge density transferred uniformly within the PVDF:PZT-N hybrid nanofibers during contact and separation of opposite charge surfaces.[58,59]

The device area of the TENG-PENG has produced a significant influence on output voltage and current. Consequently, we designed single-dielectric TENG-PENG devices with three different effective areas of 1 × 1 cm^2, 2 × 2 cm^2, and 5 × 5 cm^2 by using optimum PVDF:PZT-N hybrid nanofiber mat. The area-dependent output voltage with respect to time is shown in Figure 6a. In 1 cm^2 device, the output voltage increased from 2.64 V in the tribo region to 4.24 V in the coupled triboelectric and piezoelectric regions. For the 4 cm^2 device, the output voltage reached 3.26 V in the triboelectric region and gradually increased to 9.16 V in the coupled triboelectric and piezoelectric regions. Notably, the 25 cm^2 device exhibited a triboelectric region output voltage of 9.2 V, increasing to 22.5 V in the coupled triboelectric and piezoelectric regions. Further, Figure 6b shows the output voltage dependence corresponds to device area of the TENG-PENG, highlighting the significant impact of the effective device area on the output voltage performance. The area-dependent output current with respect to time is shown in Figure 6c. A device area of 1 cm^2 exhibited an increase in the output current from 1.17×10^{-7} A for the triboelectric region to 2.6×10^{-7} A for the coupled triboelectric and piezoelectric regions. Further, the output current for 4 cm^2 exhibits 4.97×10^{-7} A for the triboelectric region, and gradually increases to 6.6×10^{-7}A for the coupled triboelectric and piezoelectric regions. However, the output current of 5.67×10^{-7} A, shown for 25 cm^2 in the triboelectric region, increases to 9.9×10^{-7} A for the coupled triboelectric and piezoelectric regions. Figure 6d shows the dependence of the output current on the device area of a single-dielectric TENG-PENG device.

In the double-dielectric TENG-PENG structure, we introduced another electropositive dielectric layer consisting of a PVA thin film underneath the upper copper sheet acting as a single electropositive electrode, as shown in Figure 7a. The operational cycle consists of four stages similar as discussed for single dielectric TENG-PENG device, as depicted in Figure 7b. The open/released state demonstrated stage 1, where a narrow air gap of ∼2.5 cm between the electropositive PVA coated upper copper electrode layer and the electronegative PVDF:PZT-N nanofiber layers. Here, the dipoles within the nanofibers are disoriented resulting in no potential difference, leading to no charge transfer. Further, the device enters to stage 2 in proximity state during gentle manual tapping. The upper electropositive copper sheet with PVA comes into close proximity to electronegative PVDF:PZT-N nanofiber layers, which leads to the development of opposite charges due to contact electrification. Further, due to electrostatic induction, few electrons move from the bottom copper electrode to the upper copper electrode and produce potential difference. Overall, transfer of electrons occurs due to the triboelectric effect generating an output pulse.[60] However, after exerting complete mechanical pressure, the device enters into stage 3. The upper PVA thin film with copper sheet come into full contact with the PVDF:PZT-N nanofiber layers and experienceing stress. The piezoelectric effect induces electric polarization within the PVDF:PZT-N nanofibers and their dipoles are almost completely aligned. This leads to the transfer of maximum charge carriers from the bottom copper electrode to the upper copper electrode. Thus, the output pulse is enhanced due to triboelectric and piezoelectric effects, which are superimposed.[61,62] During the releasing stage, electrostatic induction induces electron flow in the opposite direction between the two electrodes to equalize the potential, enabling electron transfer from the upper copper electrode to the bottom copper electrode, consequently generating a negative output pulse.[51] Subsequently, charge neutralization occurs between the electrodes after complete separation from the triboelectric and piezoelectric effects. Finally, the device returns to the initial stage of the open/released state with disoriented dipoles. The notable area-dependent output voltages of the double-dielectric TENG-PENG devices with three different effective areas of 1 × 1 cm^2, 2 × 2 cm^2, and 5 × 5 cm^2 are shown in Figure 7c. For the 1 cm^2 device, the output voltage increased from 5.01 V in the triboelectric region to 10.24 V in the combined triboelectric and piezoelectric regions. In the case of the 4 cm^2 device, the output voltage peaked at 12.26 V in the triboelectric region, steadily increasing to 20.3 V in the combined triboelectric and piezoelectric regions. Remarkably, the 25 cm^2 device exhibited a triboelectric region output voltage of 20.15 V, increasing to 40.2 V in the combined triboelectric and piezoelectric regions. Figure 7d illustrates the dependency of the output voltage on the area of the double-dielectric TENG-PENG devices, emphasizing the notable influence of the device area on its performance characteristics. In addition, Figure 7e depicts the output current, showcasing the variation in the output current with respect to the device area. The 1 cm^2 device area exhibited an output current that increased from 3.17×10^{-7} A in the triboelectric region to 8.36×10^{-7} A in the coupled triboelectric and piezoelectric regions. Similarly, for the 4 cm^2 device, the output current started at 3.17×10^{-7} A in the triboelectric region and gradually increased to 2.67×10^{-6}A in the combined triboelectric and piezoelectric regions. In contrast, the 25 cm^2 device showed an output current of 3.78×10^{-6} A in the triboelectric region, which increased to 6.98×10^{-6}A in the combined triboelectric and piezoelectric regions. Figure 7f illustrates the dependence of the maximum output current on the area of the double-dielectric TENG-PENG device, emphasizing the notable influence of the device area on its performance characteristics. The rectified voltage for each area-dependent device is depicted in Figure S7. Moreover, the kinetics of the coupled triboelectric and piezoelectric responses are explained through a single-pulse output voltage corresponding to each state, as depicted in Figure S8, and the fabricated area-dependent double-dielectric TENG-PENG devices with their cross sections are shown in Figure S9. The increase in the effective contact surface area increases the electrical output performance as it augments the charge accumulation on the contact area, thus increasing the charge transfer between the oppositely charged layers, consequently increasing the output voltage and current.[63] In summary, the double-dielectric PENG-TENG device structure seems to offer greater promise for generating a higher output

https://doi.org/10.1021/acsanm.4c02292
ACS Appl. Nano Mater. 2024, 7, 15425−15437

voltage and current compared to the single-dielectric device structure when PVDF:PZT-N hybrid nanofibers are used. A comparative study of single-dielectric TENG-PENG with different composite materials and double-dielectric TENG-PENG is presented in Table 1.

Table 1. Comparative Study of the Output Responses for Different Coupled TENG-PENG Devices Based on the Composite Nanofibers Development

fabricated device	developed materials	TENG-PENG voltage (V)	TENG-PENG current
single dielectric	PVDF	3.9	40 nA
	PVDF:PZT	4	90 nA
	PVDF:PZT-N	22	1 μA
double dielectric	PVDF:PZT-N	40	7 μA

3.6. Mechanical Property Analysis. The stability of mechanical properties is a crucial factor in analyzing the mechanical energy stored in polymers or composite materials. Figure 8a demonstrates the storage modulus of PVDF:PZT-N compared to PVDF:PZT and PVDF. The storage modulus of PVDF:PZT-N surpasses those of PVDF:PZT and pure PVDF, reaching approximately 306 Pa. This proves that the PVDF:PZT-N polymer maintains exceptional stability with a highly elastic behavior under extreme deformation, imparting superior mechanical energy storage properties. Additionally, Nafion serves as an excellent cross-linker between PVDF and PZT molecules, effectively functioning as a viscoelastic solid. Furthermore, the strength and stiffness of the nanofibers were investigated using tensile strength measurement. The tensile strengths of PVDF, PVDF:PZT composite, and PVDF:PZT-N hybrid nanofibers were analyzed using stress−strain curves, as depicted in Figure 8b. It is evident from the observed stress−strain curves that the PVDF:PZT-N hybrid nanofibers exhibit significantly higher tensile strength than the PVDF:PZT composite and PVDF nanofibers. The inset stress−strain curves corresponding to the yield points of PVDF, PVDF:PZT, and PVDF:PZT-N nanofibers are ~0.51, ~1.06, and ~1.48 MPa, respectively, as observed from the tangent plot. Moreover, the fracture points for pure PVDF, PVDF:PZT, and PVDF:PZT-N nanofibers lie at ~3.38, ~5.53, and ~6.31 MPa, respectively. This demonstrates that the strength of the PVDF:PZT-N hybrid nanofibers is nearly twice that of the pure PVDF nanofibers. The enhanced strength and stiffness of the PVDF:PZT-N hybrid nanofibers could be attributed to the combined effect of the strong interface interaction of the PZT nanoparticles and Nafion with the PVDF polymer.[64] Additionally, the excellent tensile strength of the hybrid nanofibers results from the improved dispersion of PZT within the PVDF:PZT-N matrix.[65] The superior mechanical elastic characteristics of PVDF:PZT-N are considerable for flexible and stretchable materials, particularly in applications involving PENG and TENG devices that demand elastic materials.

The bridge-rectifier circuit diagram is implemented, as shown in Figure 9a, and designed on the breadboard with a TENG-PENG device interconnected with LEDs and a segment display board, as shown in Figure 9b. Consistent manual tapping of the TENG-PENG device generates an alternating current (AC) signal. The bridge rectifier circuit converts the AC signal into direct current (DC), which illuminated the display board showing number "seven", multiple green LED, and IITM LED display board, as shown in Figure 9c,9d,9e respectively. Moreover, a movie of flashing LEDs and displays is attached to a video file (Supporting Material). This energy conversion process is facilitated by the generation of charges, their separation, and the flow of charges between the copper sheets, PVA sheets, and PVDF:PZT-N nanofiber mat.[66]

4. CONCLUSIONS

In conclusion, our study successfully demonstrated the fabrication of well-dispersed Nafion-incorporated PVDF:PZT hybrid nanofibers, exhibiting a remarkable enhancement in the β phase compared to bare PVDF nanofibers. The PVDF:PZT-N hybrid nanofibers exhibited an impressive increase in surface potential, reaching approximately 175 mV. These hybrid nanofibers were utilized in the construction of a single-dielectric layer TENG-PENG, where the synergistic effects of triboelectricity and piezoelectricity significantly boost the output voltage and current, recorded 22.5 V and 1 μA, respectively. Subsequently, a remarkable enhancement in the double-dielectric TENG-PENG device was observed for the maximum output voltages and currents of 40 V and 7 μA, respectively. Furthermore, the elastic threshold of the PVDF:PZT-N nanofibers exhibited noteworthy progress to 1.48 MPa. However, certain limitations of PVDF:PZT

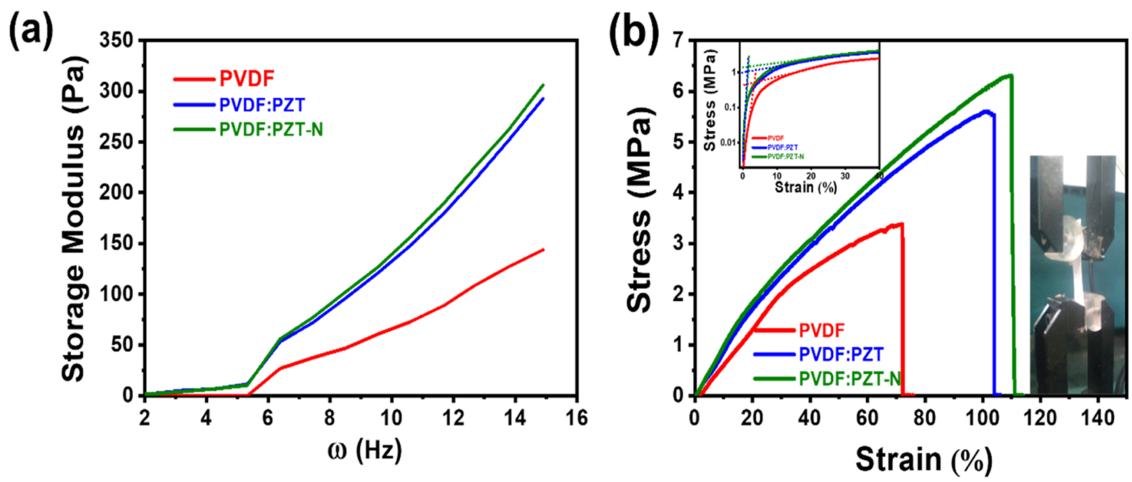

Figure 8. (a) Storage modulus versus frequency and (b) stress−strain curves of PVDF, PVDF:PZT, and PVDF:PZT-N nanofibers.

https://doi.org/10.1021/acsanm.4c02292
ACS Appl. Nano Mater. 2024, 7, 15425−15437

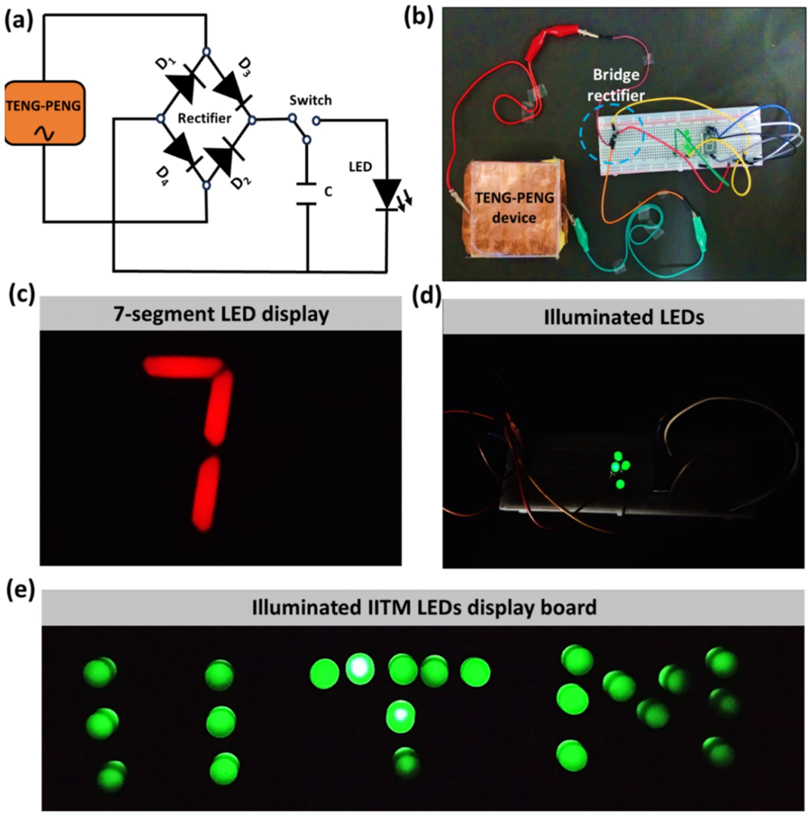

Figure 9. (a) Bridge-rectifier circuit diagram, (b) TENG-PENG device connections with LEDs and display boards, (c) flashing seven-segment LED display board, (d) picture of the illuminated LEDs, and (e) powering IITM LED display board.

composite nanofibers unveil challenges in achieving uniform PZT dispersion, limited frequency response, and meager vibration capture, which hinder their widespread adoption in nanogenerators. Moreover, PVDF:PZT-N nanofibers reinforced with flexible and stable Nafion demonstrated the capability of illuminating multiple LEDs through manual tapping. This innovative TENG-PENG technology introduces exciting prospects for propelling advancements in mechanical energy harvesting, thereby facilitating the pursuit of sustainable solutions for powering underwater wireless sensors and biomedical applications.

■ ASSOCIATED CONTENT

Supporting Information

The Supporting Information is available free of charge at https://pubs.acs.org/doi/10.1021/acsanm.4c02292.

Flashing LEDs and seven-segment LED display board (MP4)

Varied concentrations of PZT in the PVDF:PZT solution, concentration variation of Nafion in the PVDF:PZT-N composite solution, FTIR spectra of the PVDF:PZT-N, SEM images, Raman mapping, XRD spectra of the pure glass substrate, area-dependent rectified voltage, coupled triboelectric and piezoelectric output rectified voltages at single pulse, and area-dependent TENG-PENG devices (PDF)

■ AUTHOR INFORMATION

Corresponding Author

Ranbir Singh − *School of Mechanical and Materials Engineering (SMME), Indian Institute of Technology Mandi (IIT Mandi), Mandi, Himachal Pradesh 175005, India;* orcid.org/0000-0002-5659-478X; Email: ranbir@iitmandi.ac.in

Authors

Saira Bano − *School of Mechanical and Materials Engineering (SMME), Indian Institute of Technology Mandi (IIT Mandi), Mandi, Himachal Pradesh 175005, India*

Bablesh Gupta − *School of Mechanical and Materials Engineering (SMME), Indian Institute of Technology Mandi (IIT Mandi), Mandi, Himachal Pradesh 175005, India*

Satinder K. Sharma − *School of Computing and Electrical Engineering (SCEE), Indian Institute of Technology Mandi (IIT Mandi), Mandi, Himachal Pradesh 175005, India;* orcid.org/0000-0001-9313-5550

Complete contact information is available at: https://pubs.acs.org/10.1021/acsanm.4c02292

Notes

The authors declare no competing financial interest.

■ ACKNOWLEDGMENTS

The authors gratefully acknowledge the financial support (Seed Grant from IIT Mandi) and the experimental facility provided by C4DFED & AMRC at IIT Mandi.

■ REFERENCES

(1) Wang, Y.; Yang, Y.; Wang, Z. Triboelectric nanogenerators as flexible power sources. *npj Flexible Electron.* **2017**, *1* (1), No. 10.

(2) Maria Joseph Raj, N. P.; Alluri, N.; Vivekananthan, V.; Chandrasekhar, A.; Khandelwal, G.; Kim, S. J. Sustainable yarn

type-piezoelectric energy harvester as an eco-friendly, cost-effective battery-free breath sensor. *Appl. Energy* **2018**, *228*, 1767−1776.

(3) Wang, Z. L. Triboelectric nanogenerators as new energy technology for self-powered systems and as active mechanical and chemical sensors. *ACS Nano* **2013**, *7* (11), 9533−9557.

(4) Zhu, J.; Zhu, M.; Shi, Q.; Wen, F.; Liu, L.; Dong, B.; Haroun, A.; Yang, Y.; Vachon, P.; Guo, X.; He, T.; Lee, C. Progress in TENG technology—A journey from energy harvesting to nanoenergy and nanosystem. *EcoMat* **2020**, *2* (4), No. e12058.

(5) Matthews, J. O.; Silverman, J. C.; Mosti, V. A.; Manalo, J. Devices for energy harvesting and storage. Google Patents: 2018.

(6) Min, G.; Khandelwal, G.; Dahiya, A. S.; Mulvihill, D. M.; Dahiya, R. Integrated piezo-triboelectric nanogenerators based self-powered flexible temperature and pressure sensor. *IEEE J. Flexible Electron.* **2023**, *2* (2), 84−91.

(7) Guo, Y.; Zhang, H.; Zhong, Y.; Shi, S.; Wang, Z.; Wang, P.; Zhao, Y. Triboelectric nanogenerator-based near-field electrospinning system for optimizing PVDF fibers with high piezoelectric performance. *ACS Appl. Mater. Interfaces* **2023**, *15* (4), 5242−5252.

(8) Li, X.; Yu, W.; Gao, X.; Liu, H.; Han, N.; Zhang, X. PVDF microspheres@ PLLA nanofibers-based hybrid tribo/piezoelectric nanogenerator with excellent electrical output properties. *Mater. Adv.* **2021**, *2* (18), 6011−6019.

(9) Li, M.; Lu, H. W.; Wang, S. W.; Li, R. P.; Chen, J. Y.; Chuang, W. S.; Yang, F. S.; Lin, Y. F.; Chen, C. Y.; Lai. Filling the gap between topological insulator nanomaterials and triboelectric nanogenerators. *Nat. Commun.* **2022**, *13* (1), No. 938.

(10) Wu, J.; Zheng, Y.; Li, X. Recent progress in self-powered sensors based on triboelectric nanogenerators. *Sensors* **2021**, *21* (21), 7129.

(11) Shanbedi, M.; Ardebili, H.; Karim, A. Polymer-based triboelectric nanogenerators: Materials, characterization, and applications. *Prog. Polym. Sci.* **2023**, *144*, No. 101723.

(12) Zhang, C.; Sun, H.; Zhu, Q. Preparation and property enhancement of poly (Vinylidene Fluoride)(PVDF)/lead zirconate titanate (PZT) composite piezoelectric films. *J. Electron. Mater.* **2021**, *50*, 6426−6437.

(13) Yan, Z.; Zaïri, F.; Zaoui, A. Multiscale modeling of the strain-induced $\alpha \rightarrow \beta$ phase transition and piezoelectric activity in semi-crystalline poly (vinylidene fluoride) over a large-strain range. *Mech. Mater.* **2023**, *182*, No. 104666.

(14) Itoh, A.; Takahashi, Y.; Furukawa, T.; Yajima, H. Solid-state calculations of poly (vinylidene fluoride) using the hybrid DFT method: spontaneous polarization of polymorphs. *Polym. J.* **2014**, *46* (4), 207−211.

(15) Zhou, J.; Hou, D.; Cheng, S.; Zhang, J.; Chen, W.; Zhou, L.; Zhang, P. Recent advances in dispersion and alignment of fillers in PVDF-based composites for high-performance dielectric energy storage. *Mater. Today Energy* **2023**, *31*, No. 101208.

(16) Yang, L.; Wang, H.; Fang, S.; Li, M. Research progress on energy storage performance enhancement strategies for polyvinylidene fluoride-based composites. *J. Alloys Compd.* **2023**, *960*, No. 170831.

(17) Cheng, L.; Xu, Q.; Zheng, Y.; Jia, X.; Qin, Y. A self-improving triboelectric nanogenerator with improved charge density and increased charge accumulation speed. *Nat. Commun.* **2018**, *9* (1), No. 3773.

(18) Zhang, Y.; Zhang, Y.; Xue, X.; Cui, C.; He, B.; Nie, Y.; Deng, P.; Wang, Z. PVDF−PZT nanocomposite film based self-charging power cell. *Nanotechnology* **2014**, *25* (10), No. 105401.

(19) Wang, X.; Yang, B.; Liu, J.; Zhu, Y.; Yang, C.; He, Q. A flexible triboelectric-piezoelectric hybrid nanogenerator based on P (VDF-TrFE) nanofibers and PDMS/MWCNT for wearable devices. *Sci. Rep.* **2016**, *6* (1), No. 36409.

(20) Zhang, T.; Sun, H.; Yin, C.; Jung, Y. H.; Min, S.; Zhang, Y.; Zhang, C.; Chen, Q.; Lee, K. J.; Chi, Q. Recent progress in polymer dielectric energy storage: From film fabrication and modification to capacitor performance and application. *Prog. Mater. Sci.* **2023**, *140*, No. 101207.

(21) Chen, J.; Ayranci, C.; Tang, T. Piezoelectric performance of electrospun PVDF and PVDF composite fibers: a review and machine learning-based analysis. *Mater. Today Chem.* **2023**, *30*, No. 101571.

(22) Selleri, G.; Gino, M. E.; Brugo, T. M.; D'Anniballe, R.; Tabucol, J.; Focarete, M. L.; Carloni, R.; Fabiani, D.; Zucchelli, A. Self-sensing composite material based on piezoelectric nanofibers. *Mater. Des.* **2022**, *219*, No. 110787.

(23) Purushothaman, S. M.; Tronco, M. F.; Kottathodi, B.; Royaud, I.; Ponçot, M.; Kalarikkal, N.; Thomas, S.; Rouxel, D. A review on electrospun PVDF-based nanocomposites: Recent trends and developments in energy harvesting and sensing applications. *Polymer* **2023**, *283*, No. 126179.

(24) Lu, L.; Ding, W.; Liu, J.; Yang, B. Flexible PVDF based piezoelectric nanogenerators. *Nano Energy* **2020**, *78*, No. 105251.

(25) Tzou, H.; Ye, R. Pyroelectric and thermal strain effects of piezoelectric (PVDF and PZT) devices. *Mech. Syst. Signal Process.* **1996**, *10* (4), 459−469.

(26) Li, P.; Jiang, W.; Lu, R.; Yuan, D.; Shan, J.; Xiao, J. Design and durability of PZT/PVDF composites based on pavement perception. *Constr. Build. Mater.* **2022**, *323*, No. 126621.

(27) Zeng, Z.; Yu, D.; He, Z.; Liu, J.; Xiao, F. X.; Zhang, Y.; Wang, R.; Bhattacharyya, D.; Tan, T. Graphene oxide quantum dots covalently functionalized PVDF membrane with significantly-enhanced bactericidal and antibiofouling performances. *Sci. Rep.* **2016**, *6* (1), No. 20142.

(28) Fang, J.; Wang, K.; Bohringer, K. Self-assembly of PZT actuators for micropumps with high process repeatability. *J. Microelectromech. Syst.* **2006**, *15* (4), 871−878.

(29) Kang, D. H.; Kang, H. W. Surface energy characteristics of zeolite embedded PVDF nanofiber films with electrospinning process. *Appl. Surf. Sci.* **2016**, *387*, 82−88.

(30) Wankhade, S. H.; Tiwari, S.; Gaur, A.; Maiti, P. PVDF−PZT nanohybrid based nanogenerator for energy harvesting applications Applied Surface Science. *Energy Rep.* **2020**, *6*, 358−364.

(31) Asghar, A. H.; Qaseem, A.; Alam, W.; Akhtar, M. In *Synergistic improvement in piezoelectric, electrical, and mechanical properties of PVDF/PZT/Clay based Hybrid Nanocomposites*, 2022 19th International Bhurban Conference on Applied Sciences and Technology (IBCAST); IEEE, 2022; pp 1−9.

(32) Gadim, T. D.; Vilela, C.; Loureiro, F. J.; Silvestre, A. J.; Freire, C. S.; Figueiredo, F. M. Nafion and nanocellulose: A partnership for greener polymer electrolyte membranes. *Ind. Crops Prod.* **2016**, *93*, 212−218.

(33) Li, W.; Lu, L.; Yan, F.; Palasantzas, G.; Loos, K.; Pei, Y. High-performance triboelectric nanogenerators based on TPU/mica nanofiber with enhanced tribo-positivity. *Nano Energy* **2023**, *114*, No. 108629.

(34) Xu, C.; Zhang, L.; Xu, Y.; Yin, Z.; Chen, Q.; Ma, S.; Zhang, H.; Huang, R.; Zhang, C.; Jin, L.; et al. Filling the holes in piezopolymers with a solid electrolyte: a new paradigm of poling-free dynamic electrets for energy harvesting. *J. Mater. Chem. A* **2017**, *5* (1), 189−200.

(35) Hou, L.; Huan, Y.; Zheng, M.; Liu, Y.; Wang, C.; Wang, X.; Li, C.; Wang, Z.; Wei, T. 3D vertically aligned microchannel structure to enhance piezoelectric energy harvesting performance of PZT/PVDF&CNTs piezoelectric composites *J. Materiomics* 2023, DOI: 10.1016/j.jmat.2023.11.006.

(36) Yan, J.; Liu, M.; Jeong, Y. G.; Kang, W.; Li, L.; Zhao, Y.; Deng, N.; Cheng, B.; Yang, G. Performance enhancements in poly (vinylidene fluoride)-based piezoelectric nanogenerators for efficient energy harvesting. *Nano Energy* **2019**, *56*, 662−692.

(37) Li, J.; Zhou, G.; Hong, Y.; He, W.; Wang, S.; Chen, Y.; Wang, C.; Tang, Y.; Sun, Y.; Zhu, Y. Highly sensitive, flexible and wearable piezoelectric motion sensor based on PT promoted β-phase PVDF. *Sens. Actuators, A* **2022**, *337*, No. 113415.

(38) Singh, P.; Borkar, H.; Singh, B.; Singh, V.; Kumar, A. Ferroelectric polymer-ceramic composite thick films for energy storage applications. *AIP Adv.* **2014**, *4* (8), No. 087117.

(39) Du, X.; Zhou, Z.; Zhang, Z.; Yao, L.; Zhang, Q.; Yang, H. Porous, multi-layered piezoelectric composites based on highly oriented PZT/PVDF electrospinning fibers for high-performance piezoelectric nanogenerators. *J. Adv. Ceram.* **2022**, *11*, 331−344.

(40) Liu, K.; Wang, H.; Wu, Y.; Wang, Y.; Yuan, C. Preparation and properties of gamma-PVDF/lead zirconium titanate composites. *Polymer* **2023**, *281*, No. 126091.

(41) Kaur, N.; Bahadur, J.; Panwar, V.; Singh, P.; Rathi, K.; Pal, K. Effective energy harvesting from a single electrode based triboelectric nanogenerator. *Sci. Rep.* **2016**, *6* (1), No. 38835.

(42) Koç, M.; Paralı, L.; Şan, O. Fabrication and vibrational energy harvesting characterization of flexible piezoelectric nanogenerator (PEN) based on PVDF/PZT. *Polym. Test.* **2020**, *90*, No. 106695.

(43) Zhang, J. H.; Zhang, Y.; Sun, N.; Li, Y.; Du, J.; Zhu, L.; Hao, X. Enhancing output performance of triboelectric nanogenerator via large polarization difference effect. *Nano Energy* **2021**, *84*, No. 105892.

(44) Feng, Y.; Deng, Q.; Peng, C.; Wu, Q. High dielectric and breakdown properties achieved in ternary BaTiO3/MXene/PVDF nanocomposites with low-concentration fillers from enhanced interface polarization. *Ceram. Int.* **2019**, *45* (6), 7923−7930.

(45) Liu, X. F.; Xiong, C. X.; Sun, H. J.; Dong, L. J.; li, R.; Liu, Y. Piezoelectric and dielectric properties of PZT/PVC and graphite doped with PZT/PVC composites. *Mater. Sci. Eng.* **2006**, *127* (2−3), 261−266.

(46) Zak, A. K.; Gan, W. C.; Majid, W. A.; Darroudi, M.; Velayutham, T. S. Experimental and theoretical dielectric studies of PVDF/PZT nanocomposite thin films. *Ceram. Int.* **2011**, *37* (5), 1653−1660.

(47) Kim, T.; Joshi, B.; Lim, W.; Samuel, E.; Aldalbahi, A.; Periyasami, G.; Lee, H. S.; An, S.; Yoon, S. S. Scalable, flexible BaTiO3/PVDF piezocomposites prepared via supersonic spraying for use in energy harvesting and integrated energy storage devices. *Nano Energy* **2023**, *115*, No. 108682.

(48) Kumar, A.; Kumar, S.; Pathak, A. K.; Ansari, A. A.; Rai, R.; Lee, Y.; Kim, S. Y.; Van Le, Q.; Singh, L. Recent progress in nanocomposite-oriented triboelectric and piezoelectric energy generators: An overview. *Nano-Struct. Nano-Objects* **2023**, *36*, No. 101046.

(49) Luo, B.; Cai, C.; Liu, T.; Zhang, S.; Gao, C.; Liu, Y.; Chi, M.; Wang, J.; Wang, S.; Nie, S. Triboelectric probes for investigating charge transfer at the colloid-solid interface. *Nano Energy* **2023**, *117*, No. 108874.

(50) Wang, X. Piezoelectric nanogenerators—Harvesting ambient mechanical energy at the nanometer scale. *Nano Energy* **2012**, *1* (1), 13−24.

(51) Yi, H.; Xiong, L. The effect of the electric field on the output performance of triboelectric nanogenerators. *J. Comput. Electron.* **2020**, *19*, 1670−1677.

(52) Kim, M. P.; Um, D. S.; Shin, Y. E.; Ko, H. High-performance triboelectric devices via dielectric polarization: a review. *Nanoscale Res. Lett.* **2021**, *16*, No. 35.

(53) Kim, M. P.; Lee, Y.; Hur, Y. H.; Park, J.; Kim, J.; Lee, Y.; Ahn, C. W.; Song, S. W.; Jung, Y. S.; Ko, H. Molecular structure engineering of dielectric fluorinated polymers for enhanced performances of triboelectric nanogenerators. *Nano Energy* **2018**, *53*, 37−45.

(54) Wu, H.; Wang, J.; Wu, Z.; Kang, S.; Wei, X.; Wang, H.; Luo, H.; Yang, L.; Liao, R.; Wang, Z. Multi-parameter optimized triboelectric nanogenerator based self-powered sensor network for broadband aeolian vibration online-monitoring of transmission lines. *Adv. Energy Mater.* **2022**, *12* (13), No. 2103654.

(55) Mahboubizadeh, S.; Dilamani, S. T.; Baghshahi, S. Piezoelectricity performance and β-phase analysis of PVDF composite fibers with BaTiO3 and PZT reinforcement. *Heliyon* **2024**, *10* (3), No. e25021.

(56) Babu, A.; Supraja, P.; Mishra, S.; Kumar, K. U.; Rakesh Kumar, R.; Kumar, R. R.; Haranath, D.; Thirmal, C.; Raju, N.; Rao, T. V.; Balaji, K. Energy harvesting properties of the Nafion thin films. *Eng. Res. Express* **2022**, *4* (4), No. 045015.

(57) Tarokh, A.; Karan, K.; Ponnurangam, S. Atomistic MD study of nafion dispersions: Role of solvent and counterion in the aggregate structure, ionic clustering, and acid dissociation. *Macromolecules* **2020**, *53* (1), 288−301.

(58) Shi, L.; Jin, H.; Dong, S.; Huang, S.; Kuang, H.; Xu, H.; Chen, J.; Xuan, W.; Zhang, S.; Li, S.; Wang, X.; Luo, J. High-performance triboelectric nanogenerator based on electrospun PVDF-graphene nanosheet composite nanofibers for energy harvesting. *Nano Energy* **2021**, *80*, No. 105599.

(59) Kumar, P.; Choudhary, S.; Sharma, K. P.; Sharma, S. K.; Singh, R.; Singh, R. Light-Sensitive PVDF-TrFE: PDI Hybrid Nanofibers-Based Flexible Bimodal Piezoelectric Nanogenerator. *IEEE J. Flexible Electron.* **2022**, *1* (3), 194−202.

(60) Hu, D.; Yao, M.; Fan, Y.; Ma, C.; Fan, M.; Liu, M. Strategies to achieve high performance piezoelectric nanogenerators. *Nano energy* **2019**, *55*, 288−304.

(61) Gopal, S. R.; Velayutham, T.; Gan, W.; Cheong, J.; Soh, A. A hybrid piezoelectric and triboelectric nanogenerator with lead-free BZT−BCT/PDMS composite and PVA film for scavenging mechanical energy. *RSC Adv.* **2023**, *13* (12), 7921−7928.

(62) Bai, P.; Zhu, G.; Zhou, Y. S.; Wang, S.; Ma, J.; Zhang, G.; Wang, Z. L. Dipole-moment-induced effect on contact electrification for triboelectric nanogenerators. *Nano Res.* **2014**, *7*, 990−997.

(63) Yang, W.; Wang, X.; Li, H.; Wu, J.; Hu, Y.; Li, Z.; Liu, H. Fundamental research on the effective contact area of micro-/nano-textured surface in triboelectric nanogenerator. *Nano Energy* **2019**, *57*, 41−47.

(64) Shehata, N.; Nair, R.; Boualayan, R.; Kandas, I.; Masrani, A.; Elnabawy, E.; Omran, N.; Gamal, M.; Hassanin, A. H. Stretchable nanofibers of polyvinylidenefluoride (PVDF)/thermoplastic polyurethane (TPU) nanocomposite to support piezoelectric response via mechanical elasticity. *Sci. Rep.* **2022**, *12* (1), No. 8335.

(65) Yuan, C.; Zhang, C.; Yang, C.; Wu, F.; Xiao, S.; Sun, H. Enhanced Piezoelectric Properties of Poly (Vinylidene Fluoride)/Lead Zirconate Titanate (PVDF/PZT) Fiber Films Fabricated by Electrospinning. *J. Electron. Mater.* **2023**, *52* (11), 7193−7207.

(66) Kang, X.; Pan, C.; Chen, Y.; Pu, X. Boosting performances of triboelectric nanogenerators by optimizing dielectric properties and thickness of electrification layer. *RSC Adv.* **2020**, *10* (30), 17752−17759.

https://doi.org/10.1021/acsanm.4c02292
ACS Appl. Nano Mater. 2024, 7, 15425−15437